

## Chapter 1: Introduction



Bose statistics were first developed in 1924 to describe the quantum behavior of photons [1], quanta of light with integer valued spin. Today, we routinely produce atomic Bose-Einstein condensates in the laboratory and even use them as a platform for the analog simulation of complex systems. The field has certainly come a long way!



Bose-Einstein condensation (BEC) in atomic gases was observed for the first time in 1995 in dilute vapors of  $^{87}\text{Rb}$  [2] and  $^{23}\text{Na}$  [3]. Even though the BEC phase had been predicted for a long time it wasn't until experimental techniques of laser cooling and trapping were developed that bosonic atoms were cooled down to temperatures low enough for condensation to occur<sup>1</sup>. The experimental realization of this new phase of matter opened new possibilities for studying macroscopic quantum phenomena such as the propagation of collective modes [5, 6] and interference of coherent matter waves [7] and jump-started an ever growing field of research. For this achievement Eric Cornell, Carl Wieman and Wolfgang Ketterle were awarded the 2001 Nobel Prize in physics.

It has been more than 20 years (and many more in the learning of atomic physics) and the field of quantum degenerate gases has expanded to include degenerate Fermi gases [8] and spinor gases [9]. As the field continues to grow, new control and detection techniques are being constantly developed, enabling the use of BECs and ultracold atomic systems in general not just as an object of study by themselves but as tools for a wide range of scientific endeavors, from precision measurements [10] to the analog simulation of complex systems.

Quantum degenerate gases have proven to be an ideal platform for quantum simulation [11]. A very straightforward example comes from the use of optical lattices, where the periodic potential imparted by standing waves of light serves as an analogue to the crystal structure in a solid. Perhaps the first iconic realization of a quantum simulation was the study of the Bose-Hubbard model in three-dimensional optical lattices [12], the bosonic analogue of a model which is believed to be relevant to high- $T_c$  superconductors.

The development of light induced gauge-fields [13] has been another important milestone in the field of quantum simulation. Such fields can be used to mimic the effect of magnetic [14, 15] and electric [16] fields with potential applications to the realization of quantum Hall materials with large magnetic fluxes [14, 17] and fractional quantum Hall states [18]. Furthermore, light-induced gauge fields

---

<sup>1</sup>For a more in depth story of the BEC field I highly recommend reading [4].

can be used to engineer spin-orbit coupling interactions [19] as those present in two-dimensional materials, a necessary ingredient for the spin quantum Hall effect and certain kinds of topological insulators [20]. Chapter 8 will focus on a new implementation of Rashba-type spin-orbit [21, 22] coupling in an ultracold  $^{87}\text{Rb}$  atoms.

The precise level of control and tunability of ultracold atomic systems allow us to readily implement important physical models in the laboratory. Furthermore, we can go beyond conventional materials existing in nature, and thereby create new exotic atomic ‘materials’, with interaction-dominated or topologically non-trivial band structures that can help deepen our understanding of the physical consequences of these effects on materials.

This thesis focuses on the development of new tools for the characterization and control of engineered quantum systems, and applies them to create and characterize a topological system with Rashba-type spin-orbit coupling.

The creation of new engineered systems requires the ability to characterize their single particle energies. We developed a Fourier transform spectroscopy technique which allows us to probe the single particle spectrum, and thereby verify our quantum engineering, by only looking at quantum coherent evolution.

Atomic systems are susceptible to environmental noise, leading to undesired effects such as the loss of coherence. In particular laboratories such as ours greatly suffer from noise in ambient magnetic fields and go through great efforts to diminish their effects. We implemented continuous dynamical decoupling (CDD) on a set of internal atomic states which renders them first order insensitive to changes in magnetic field, effectively turning them into clock states. These CDD states are not just a robust basis for performing experiments, they additionally gave us access to new matrix elements which were essential for the engineering of the Rashba Hamiltonian as well as other novel lattice systems [23] not presented in this thesis.

The engineering of Rashba spin-orbit coupling is certainly condensed matter inspired. However, part of the beauty of our system is we can depart from conventional materials, for example, by considering a system with Rashba SOC but without an underlying crystalline structure. We do so in the last part of this thesis and find that our conventional understanding of the topology of Bloch bands is defied by measuring half-integer valued topological invariants.

## 1.1 Thesis overview

This thesis describes both the standard experimental control and measurement techniques used to create BECs of  $^{87}\text{Rb}$  as well as new techniques developed in our lab that were applied to the engineering of Rashba spin-orbit coupling.

Chapter 2 describes the basic theory of Bose-Einstein condensation in dilute gases. I focus on the properties of gases confined to harmonic potentials and their density and momentum distributions as they are most relevant to the experiments presented here.

Chapter 3 describes the basic properties of Alkali atoms and their interactions

with magnetic and electric fields which are used as standard tools for the creation, manipulation and detection of ultracold atomic systems.

Chapter 4 summarizes the experimental apparatus where all the experiments were performed. It additionally mentions the most important upgrades to the apparatus that were not reported previously.

Chapter 5 describes a Fourier transform spectroscopy technique that exploits the relation between quantum coherent evolution and the underlying spectrum of a system and that was used to characterize experiments described later in the thesis.



Chapter 6 describes an implementation of continuous dynamical decoupling using a strong radio-frequency magnetic field that helped to both make our system more robust against environmental magnetic field noise and also allowed us to couple the internal states of the atoms in new ways that were not possible before, opening the path for new kinds of quantum simulations described in Chapters 8.

Chapter 7 presents basic concepts of topology in physics and its application to the band theory of solids. These concepts will be important for a better understanding of the topological properties of our Rashba spin-orbit coupled system.

Chapter 8 I describes a new experimental realization of Rashba spin-orbit coupling using a combination of laser beams that couple a set of CDD states. The system described in this chapter has a topological dispersion relation but no underlying crystalline structure which allows for topological invariants to take non-integer values.



## Chapter 2: Overview of Bose-Einstein condensation

 Bose-Einstein condensation (BEC) is a quantum state of matter in which particles with integer valued spin all tend to occupy or ‘condense’ into the ground state. In dilute gases, condensation occurs when the temperature of the system goes below a critical temperature where the bosons become indistinguishable particles and quantum statistics become relevant. 

BECs enable the observation of macroscopic quantum phenomena and there have been a number of fascinating experiments studying the properties of these systems, from measuring interference fringes of a macroscopic wave function to studying collective effects such as the propagation of sound [4], as well as extensive theoretical developments [24]. In our experiments however BECs are not the primary object of study, instead they are used as a platform enabling the simulation of analogue physical systems.

In this Chapter I give an overview of Bose-Einstein condensation in dilute atomic gases and I describe the properties most relevant to our experiments. I start by describing the case of an ideal gas and then consider the effects of interactions and trapping potentials as are present in our case. A reader interested in learning about this subject in more depth is advised to read [25] and [26].

### 2.1 Bose-Einstein condensation of an ideal gas

At low temperatures and in thermodynamic equilibrium, the mean occupation number of non-interacting identical bosons in the state with energy  $E$  is given by the Bose-Einstein distribution

$$n(E_j) = \frac{1}{e^{(E_j - \mu)/k_B T} - 1} \quad (2.1)$$

where  $T$  is the temperature,  $\mu$  is the chemical potential (the energy cost of adding or removing a particle) and  $k_B$  is the Boltzmann constant. In the limit of large temperatures the Bose distribution can be approximated by the Maxwell-Boltzmann distribution

$$n(E_j) \approx e^{-(E_j - \mu)/k_B T} \quad (2.2)$$

which applies to classical, distinguishable particles. The chemical potential is determined by the condition that the total number of particles  $N$  is equal to the sum over all states in the distribution  $N = \sum_j n(E_j)$  and is therefore a function of  $N$  and  $T$ . Additionally, in order for  $n(E_j)$  to be positive definite we must have  $\mu \leq E_0$  where

$E_0$  is the energy of the ground state. From the Bose distribution we can see that the occupation number of the ground state is unbounded when  $\mu \rightarrow 0$  as is shown in Figure 2.1. The number of particles occupying the excited states is bounded and when that number is reached, the remaining particles can occupy the ground state and thus Bose-Einstein condensation occurs.

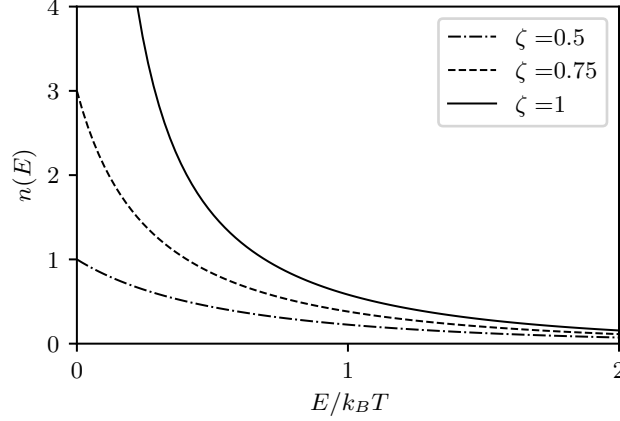


Figure 1: The Bose-Einstein distribution. Occupation number as a function of energy for different values of fugacity  $\zeta = \exp(\mu/k_B T)$ . Condensation occurs when  $\mu = 0$  ( $\zeta = 1$ ) and the occupation number in the ground state diverges.

### 2.1.1 Critical temperature

Bose-Einstein condensation can be understood in terms of the de Broglie waves associated to particles. The thermal de Broglie wavelength is defined as

$$\lambda_{\text{th}} = \left( \frac{2\pi\hbar^2}{mk_B T} \right)^{1/2} \quad (2.3)$$

and it characterized the spatial extension of the wave packet an individual particle at temperature  $T$ . Condensation occurs when  $\lambda_{\text{th}}$  becomes comparable with the inter-particle separation  $n^{-1/3}$ , where  $n = N/V$ . The quantity  $n\lambda_{\text{th}}^3$  is known as the phase space density which describes the number of particles contained in a box with volume  $\lambda_{\text{th}}^3$ .

An analytical expression for the critical temperature at which atoms condense can be derived using the Bose-Einstein distribution. For closely spaced energy levels (compared to  $k_B T$ ) the sum representing the total number of particles can be replaced by the integral

$$N = \int_0^\infty n(E)g(E)dE \quad (2.4)$$

where  $g(E)$  is the density of states and  $g(E)dE$  corresponds to the number of avail-

able states with energy between  $E$  and  $E+dE$ . For a free particle in three dimensions the density of states is

$$g(E) = \frac{Vm^{3/2}}{\sqrt{2\pi^2\hbar^2}}E^{1/2}, \quad (2.5)$$

and in general the density of states can be expressed as a power of energy  $g(E) = C_\alpha E^{\alpha-1}$ .

The integral in Equation 2.4 is not analytically solvable, however we can make the simplifying assumption  $\mu = 0$ . The critical temperature  $T_c$  is determined by the condition that all particles are in the excited states

$$\begin{aligned} N &= N_{\text{ex}}(T_c, \mu = 0) \\ &= \int_0^\infty \frac{g(E)dE}{e^{E/k_B T_c} - 1} \\ &= C_\alpha (k_B T_c)^\alpha \int_0^\infty \frac{x^{\alpha-1}}{e^x - 1} \\ &= c_\alpha (k_B T_c)^\alpha \Gamma(\alpha) \zeta(\alpha) \end{aligned} \quad (2.6)$$

where I made the substitution  $x = E/k_B T_c$ ,  $\Gamma(\alpha) = \int_0^\infty x^{\alpha-1} e^{-x} dx$  is the Gamma function and  $\zeta(\alpha) = \sum_{n=1}^\infty n^{-\alpha}$  is the Riemann zeta function. From Equation 2.6 we find that the critical temperature for Bose-Einstein condensation is

$$k_B T_c = \left( \frac{N}{C_\alpha \Gamma(\alpha) \zeta(\alpha)} \right)^{1/\alpha}. \quad (2.7)$$

If we compute the phase space density for free particles in 3D with density of states given by Equation 2.5 in combination with the expression for the critical temperature (Equation 2.6) we find that indeed when  $T = T_c$

$$n\lambda_{\text{th}}^3 = \zeta\left(\frac{3}{2}\right) \approx 2.612, \quad (2.8)$$

the inter particle spacing and the thermal wavelength are comparable. In order to experimentally produce BECs, a combination of laser and evaporative cooling techniques are deployed such that we can increase the density while minimizing the temperature and therefore maximize the phase space density. The densities for BECs of Alkali atoms typically range in of order  $10^{13}$  to  $10^{15}$  atoms/cm<sup>3</sup>.

## 2.1.2 Condensate fraction

Now we look at the fraction of particles occupying the ground state at temperatures below  $T_c$ . The total number of particles is given by  $N = N_0 + N_{\text{ex}}$ . The number of particles in the excited state will be given by the integral in Equation 2.4. For  $g(E) = C_\alpha E^{\alpha-1}$  and  $\alpha > 0$  the integral converges, we can then evaluate the integral

in Equation 2.6 for  $T < T_c$  and get

$$\begin{aligned} N_{\text{ex}} &= c_\alpha (k_B T)^\alpha \Gamma(\alpha) \zeta(\alpha) \\ &= N \left( \frac{T}{T_c} \right)^\alpha, \end{aligned} \quad (2.9)$$

where I used the fact that when  $T = T_c$  the total number  $N = N_{\text{ex}}$ . The number of particles in the ground state is therefore

$$\begin{aligned} N_0 &= N - N_{\text{ex}} \\ &= N \left[ 1 - \left( \frac{T}{T_c} \right)^\alpha \right] \end{aligned} \quad (2.10)$$

### 2.1.3 Bose gas in a harmonic trapping potential

I consider the particular case of particles confined in a three dimensional harmonic potential

$$V(\mathbf{r}) = \frac{m}{2} (\omega_x^2 x^2 + \omega_y^2 y^2 + \omega_z^2 z^2) \quad (2.11)$$

as it is the most relevant to our experiments that are performed in optical dipole traps that can be described as harmonic potentials. The density of states for is

$$g(E) = \frac{E^2}{2\hbar^2 \omega_x \omega_y \omega_z}, \quad (2.12)$$

which corresponds to  $\alpha = 3$  and  $C_3 = (2\hbar^3 \omega_x \omega_y \omega_z)^{-1}$ . Using Equation 2.6, we find that the transition temperature is

$$k_B T_c = \frac{\hbar \bar{\omega} N^{1/3}}{\zeta(3)^{1/3}} \approx 0.94 \hbar \bar{\omega} N^{1/3} \quad (2.13)$$

where  $\bar{\omega} = (\omega_x \omega_y \omega_z)^{1/3}$  is the geometric mean of the oscillation frequencies. Similarly we find that the condensed fraction is


$$N_0 = N \left[ 1 - \left( \frac{T}{T_c} \right)^3 \right] \quad (2.14)$$

Condensates in harmonic traps have some striking features that will be further explored in more detail in the following sections. The confining potential makes the BECs both finite sized and inhomogeneous which means that the BEC can be observed both in momentum space and in coordinate space. Another consequence of the inhomogeneity of these systems is the role of two-body interactions, which gets enhanced and leads to noticeable effects in measurable quantities [24, 27] such as interaction driven expansion when they are released from the confining potential. Some of these features will be discussed in more detail in the following sections.

## 2.2 Bose-Einstein condensation with atomic interactions

Even though atomic BECs are made from very dilute gases, the system is far from being an ideal gas and interactions need to be taken into account for a complete treatment.


The collisional properties of particles at low energies, such as cold atoms in a condensate, are dominated by *s*-wave scattering which can be described in terms of a single parameter the scattering length  $a$  that determines both the scattering cross section  $\sigma = 4\pi a^2$  and the phase shift of the scattered wave function.

 The magnitude of the scattering length is determined by the interatomic interaction potentials. For Alkali atoms at large distances, the two-body interactions are dominated by an attractive Van der Waals interaction  $U(r) = -C_6/r^6$  that arises from dipole-dipole interactions. At smaller distances the attractive potential is replaced by a strong repulsive electron-exchange interaction  $U(r) \rightarrow \infty$ . This minimal model captures the most important properties of the inter-atomic potential and can be solved analytically [28].

If the range of the interaction is much shorter than the mean inter-atomic distance the interaction can be approximated by an effective pseudo-potential  $U_{\text{eff}}(\mathbf{r} - \mathbf{r}')$  such that

$$a = \frac{m}{4\pi\hbar^2} \int U_{\text{eff}}(\mathbf{r} - \mathbf{r}') d\mathbf{r} \quad (2.15)$$

which determines



$$U_{\text{eff}}(\mathbf{r} - \mathbf{r}') = \frac{4\pi\hbar^2 a}{m} \delta(\mathbf{r} - \mathbf{r}') = g \delta(\mathbf{r} - \mathbf{r}'). \quad (2.16)$$

This is a nice approximation as it allows us to model the scattering between atoms as a hard sphere scattering process instead of considering the more complicated inter-atomic potentials. The sign of the scattering length determines the attractive or repulsive nature of the interactions and it plays an important role in the experimental production of BECs as it determines the rate at which atoms thermalize during evaporative cooling.

### 2.2.1 Gross-Pitaevskii equation

The full Hamiltonian describing  $N$  identical bosons with contact interactions can be written as

$$\hat{H} = \sum_{i=1}^N \left[ \frac{\mathbf{p}_i^2}{2m} + V(\mathbf{r}_i) \right] + g \sum_{i < j} \delta(\mathbf{r}_i - \mathbf{r}_j), \quad (2.17)$$

where  $V(\mathbf{r})$  is an external potential and  $\mathbf{p}_i = -i\hbar\nabla_i$  is the momentum. We now consider a normalized eigenstate of the Hamiltonian  $\Psi(\mathbf{r}_1, \mathbf{r}_2, \dots, \mathbf{r}_N)$  that satisfies the Schrödinger equation. We can simplify this state by taking a mean field approach; we assume that the system has undergone condensation so that the majority of the particles share the same single particle ground state  $\phi(\mathbf{r})$  the wavefunction can be



approximated by a symmetrized product

$$\Psi(\mathbf{r}_1, \mathbf{r}_2, \dots, \mathbf{r}_N) = \prod_{i=1}^N \phi(\mathbf{r}_i), \quad (2.18)$$

where  $\phi$  is normalized to unity. The energy of the state from Equation 2.18 is given by the expectation value

$$\begin{aligned} E &= \int \Psi^* \hat{H} \Psi d\mathbf{r} \\ &= N \int \phi^*(\mathbf{r}) \left[ -\frac{\hbar^2}{2m} \nabla^2 + V(\mathbf{r}) + \frac{(N-1)}{2} g |\phi(\mathbf{r})|^2 \right] \phi(\mathbf{r}) d\mathbf{r}, \end{aligned} \quad (2.19)$$

where  $N(N-1)/2 \approx N^2/2$  counts the number of terms in the interaction energy. Now we introduce the wave function of the condensate  $\psi(\mathbf{r}) = N^{1/2} \phi(\mathbf{r})$ , which when inserted in Equation 2.19 makes the  $N$  factors cancel out. The optimal form of  $\psi$  should minimize the energy subject to the normalization condition  $N = \int |\psi(\mathbf{r})|^2 d\mathbf{r}$ . This can be done by introducing a Lagrange multiplier  $\mu$  so that

$$\frac{\delta}{\delta \psi^*(\mathbf{r})} \left( E - \mu \int |\psi|^2 d\mathbf{r} \right) = \left[ -\frac{\hbar^2}{2m} \nabla^2 + V(\mathbf{r}) + g |\psi(\mathbf{r})|^2 - \mu \right] \psi(\mathbf{r}) = 0, \quad (2.20)$$

and we thus find that the condensate wave function obeys a non-linear Schrödinger equation known as the Gross-Pitaevskii (GP) equation.

$$\left[ -\frac{\hbar^2}{2m} \nabla^2 + V(\mathbf{r}) + g |\psi(\mathbf{r})|^2 \right] \psi(\mathbf{r}) = \mu \psi(\mathbf{r}) \quad (2.21)$$

where  $\mu$  plays the role of the chemical potential. The dynamics of the condensate will similarly be described by the time-dependent GP equation

$$i\hbar \frac{\partial}{\partial t} \psi(\mathbf{r}, t) = \left[ -\frac{\hbar^2}{2m} \nabla^2 + V(\mathbf{r}) + g |\psi(\mathbf{r}, t)|^2 \right] \psi(\mathbf{r}, t) \quad (2.22)$$

The GP equation is useful for describing the relevant phenomena associated with BECs, for example the propagation of collective excitations and the expansion of the condensate when released from a trap. The crucial assumption when deriving these equations was the mean field approximation which should be valid for dilute BECs in which the condensate fraction is close to unity. The excitations of the system can be described by a set of equations similar to those of classical hydrodynamics derived from the GP equation or alternatively using Bogoliubov theory for weakly interacting bosons [25].

## 2.2.2 Multiple component BECs

So far the discussion has been limited to single component BECs but most of our experiments are performed using a combination of multiple atomic internal states. In general, for a multiple component condensate the scattering lengths characterizing the interactions depend on the internal states of the incoming and outgoing scattering channels. Two spin- $f$ <sup>1</sup> particles colliding particles will be characterized by  $2f$  scattering lengths  $a_F$ . For bosons the total spin  $F$  takes even values and in particular for  $^{87}\text{Rb}$  atoms in the  $f = 1$  hyperfine ground state there are two scattering lengths  $a_0$  and  $a_2$  corresponding to the two-particle total angular momentum states of  $F = 0$  and  $F = 2$  respectively. The values of scattering lengths are  $a_0 = 101.8a_0$  and  $a_2 = 100.4a_0$  [9] where  $a_0 = 5.29 \times 10^{-11}$  is the Bohr radius. From the scattering lengths we can calculate two interaction coefficients

$$\begin{aligned} c_0 &= \frac{4\pi\hbar^2}{m} \frac{a_0 + 2a_2}{3} = 100.84a_0 \frac{4\pi\hbar^2}{m} \\ c_2 &= \frac{4\pi\hbar^2}{m} \frac{a_0 - a_2}{3} \approx -4.7 \times 10^{-3} c_0. \end{aligned} \quad (2.23)$$

Here  $c_0$  represents a spin-independent interaction strength that depends only on the total density while  $c_2$  is a spin-dependent energy that is relevant only where there is non-zero density of both atoms in  $m_F = \pm 1$  and is much smaller than the spin-independent energy. Similar to the case of single component BECs, the dynamics of multiple component BECs is governed by a spinor GP equation (see [9, 25]). The spin-dependent interaction strength gives rise to processes like coherent spin-mixing oscillations and domain formation and coarsening which was previously studied in the our lab [29].

The time scale at which interactions become relevant is set by the interaction energies  $n|c_i|$ . The most noticeable effect of interactions in our system is the density profile of the condensate and its anisotropic expansion after it is released from a trap which I will describe in the following sections. For the typical densities and timescales of our experiments as well as the relatively high magnetic fields that we operate at, we do not observe noticeable effects from interactions in the dynamics of the system and in the remaining chapters I will describe the dynamics of the BEC using single particle physics (i.e. the regular time-dependent Schrödinger equation).

## 2.2.3 Thomas-Fermi approximation

For systems with large  $N$ , the interaction term in the GP equation is very large compared to the kinetic energy<sup>2</sup>. As the kinetic energy becomes less important we enter the Thomas-Fermi (TF) regime where the energy of the system is given only by the external potential and the mean field energy and the GP equation is considerably

---

<sup>1</sup>Here I use the symbol  $f$  to denote the angular momentum of the individual particles and  $F$  to denote the total angular momentum of the two particles.

<sup>2</sup>It can be shown that the ratio of kinetic energy to interactions scales like  $N^{-4/5}$

simplified

$$\left[ V(\mathbf{r}) + g|\psi(\mathbf{r})|^2 \right] \psi(\mathbf{r}) = \mu\psi(\mathbf{r}). \quad (2.24)$$

In the TF regime the density distribution of the condensate  $n(\mathbf{r}) = |\psi(\mathbf{r})|^2$  reflects the shape of the external potential

$$n(\mathbf{r}) = g^{-1}[\mu - V(\mathbf{r})], \quad (2.25)$$

when  $\mu - V(\mathbf{r}) > 0$  and is otherwise zero. For a harmonic confining potential (Equation 2.11) as is typical in our experiments we find that the length scale that characterizes the size of the condensate is the Thomas-Fermi radius

$$R_j = \sqrt{\frac{2\mu}{m\omega_j^2}}, \quad j = x, y, z. \quad (2.26)$$

The density of the condensate is described by an inverted parabola

$$n(\mathbf{r}) = \frac{\mu}{g} \left( 1 - \frac{x^2}{R_x^2} - \frac{y^2}{R_y^2} - \frac{z^2}{R_z^2} \right). \quad (2.27)$$

as is shown in Figure 2a. By integrating over Equation 2.27 we find that

$$N = \frac{8\pi}{15} \frac{\mu}{g} R_x R_y R_z, \quad (2.28)$$

which allows to determine the number of atoms in the condensate based on the density profile. In practice, in-situ BECs are very dense which can lead to some technical difficulties when trying to image directly their density profiles (see Section 3.5) so instead our images are taken after the atoms are released from the trap and allowed to expand for some time. In the next section I will discuss how the density profiles of atomic clouds are modified after they are released from a confining potential.

## 2.3 Density profiles

Most ultracold atoms experiments are probed by directly imaging the atoms (e.g. with absorption imaging, Section 3.5). If the atoms are imaged in-situ we gain access to their spatial density profiles. If the atoms are released from the trap and allowed to expand in time of flight (TOF) we gain access to their momentum distribution. In this section I summarize the signatures in the density distributions of BECs and thermal atoms confined in a harmonic potential both in-situ and after TOF.

For the case of a BEC confined in a harmonic potential at zero temperature (no thermal fraction) and in the Thomas-Fermi regime discussed in Section 2.2.3,

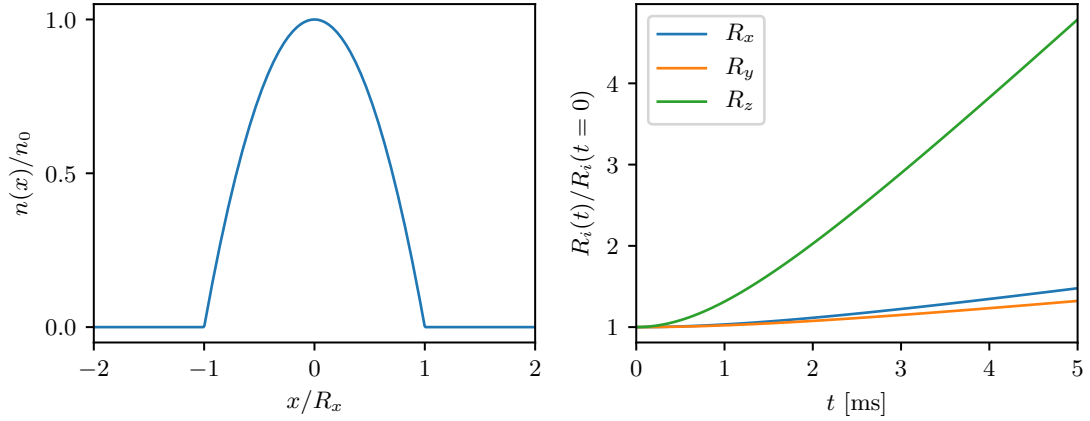


Figure 2: In the Thomas-Fermi regime where interactions are large compared to kinetic energy the density profile is determined by the external potential. **a.** Density profile along  $\mathbf{e}_x$  of a BEC in a harmonic potential. **b.** Interaction driven expansion of a BEC in time-of-flight for a trap with trapping frequencies  $(\omega_x, \omega_y, \omega_z) = 2\pi(42, 34, 133)$  Hz obtained by numerically integrating Equation 2.30.

the in-situ density distribution is described by

$$\begin{aligned} n(\mathbf{r}) &= n_0 \left( 1 - \frac{x^2}{R_x^2} - \frac{y^2}{R_y^2} - \frac{z^2}{R_z^2} \right) \\ &= \frac{15N}{8\pi R_x R_y R_z} \left( 1 - \frac{x^2}{R_x^2} - \frac{y^2}{R_y^2} - \frac{z^2}{R_z^2} \right). \end{aligned} \quad (2.29)$$

Even though the BEC is in the motional ground state, it will expand during TOF as a consequence of interactions. The expansion can be determined using the time dependent GP equation. A detail account of the procedure can be found in [27], the procedure relies on using the ansatz that the TF radii expand as

$$R_i(t) = \lambda_i(t) R_i(t=0), \quad (2.30)$$

where I assumed that the condensate is in the trap at  $t = 0$  which implies that  $\lambda_i(0) = 1$ . The trap is then suddenly turned off at  $t > 0$ . If we insert the condensate wave function with TF radii given by Equation 2.30 into the time-dependent GP equation we find a series differential equations

$$\frac{d^2 \lambda_i}{dt^2} = \frac{\omega_i^2}{\lambda_i \lambda_x \lambda_y \lambda_z} \quad (2.31)$$

which can be used to determine the density profile of the BEC in TOF. Alternatively if the density profile of the BEC is known from an image, these relations can

used to back-propagate what the original TF radii of the confined condensate was. This is helpful for example to calculate the atom number in the condensate using Equation 2.28. Figure 2b shows the scaling factors  $\lambda_i$  as a function of TOF that were obtained by numerically integrating Equation 2.30 for a harmonic potential with frequencies close to those characterizing the optical dipole trap used in the lab.

For a thermal gas in a harmonic potential at temperatures higher than the level spacing  $k_B T > \hbar \omega_{x,y,z}$  the density is given by [4]

$$n_{\text{th}}(\mathbf{r}) = \frac{1}{\lambda_{\text{th}}^3} g_{3/2}(z(\mathbf{r})) \quad (2.32)$$

where  $z(\mathbf{r}) = \exp(\mu - V(\mathbf{r})/k_B T)$ ,  $V(\mathbf{r})$  is given by Equation 2.11,  $\mu$  is the chemical potential and  $g_j(z) = \sum_i z^i / i^j$  is the Bose function. The Bose function introduces effects of quantum statistics and compared to the Maxwell-Boltzmann distribution of distinguishable particles, the peak density of a Bose gas is increased by  $g_{3/2}(z)/z$ , a phenomenon known as Bose-enhancement.

The distribution after TOF can be calculated considering that the trapped atoms fly ballistically from their position in the trap. An atom starting initially at the point  $\mathbf{r}_0$  moves to the point  $\mathbf{r}$  after a time  $t$  if its momentum is given by  $\mathbf{p} = m(\mathbf{r} - \mathbf{r}_0)/t$ , and it can be shown that

$$\begin{aligned} n_{\text{tof}} &= \frac{1}{\lambda_{\text{th}}^3} \prod_{i=1}^3 g_{3/2} \left( \exp \left[ \mu - \frac{m}{2} \sum_{i=1}^3 x_i^2 \left( \frac{\omega_i^2}{1 + \omega_i^2 t^2} \right) \right] \right) \\ &\approx \frac{1}{\lambda_{\text{th}}^3} g_{3/2} \left( \exp \left[ (\mu - \frac{mr^2}{2t^2}) / k_B T \right] \right) \end{aligned} \quad (2.33)$$

where the approximation in the second line is valid for  $t \gg \omega_i^{-1}$ . The temperature of the atoms can be estimated by looking at the wings of the density distribution after TOF. Even with the case of Bose enhancement, the density of the wings still decays exponentially as  $\exp(-x_i^2/2\sigma_i^2)$ . The temperature of the cloud can be determined using

$$\begin{aligned} k_B T &= \frac{m}{2} \left( \frac{\omega_i^2}{1 + \omega_i^2 t^2} \sigma_i^2 \right) \\ &\approx \frac{m}{2} \left( \frac{\sigma_i}{t} \right)^2 \end{aligned} \quad (2.34)$$

For partially condensed clouds the density profiles will be given by a combination of the thermal density profiles and the Thomas-Fermi density profile. Figure 3 shows the density distributions of atoms extracted from images taken after a 21 ms TOF and therefore position is mapped to momentum. The images also nicely summarize some of the main features discussed in this Chapter. Above  $T_c$  the density profile of the atoms is described by the thermal distribution (Equation 2.33). When  $T < T_c$  a small peak in the center of the thermal distribution appears indicating condensation and as temperature is decreased the fraction of atoms in the condensed



state (and therefore the height of the peak) increases. The density distribution of the condensed atoms is given by Equation 2.29, where the TF radius increases due to interactions and the scaling factors can be found using Equation 2.30.

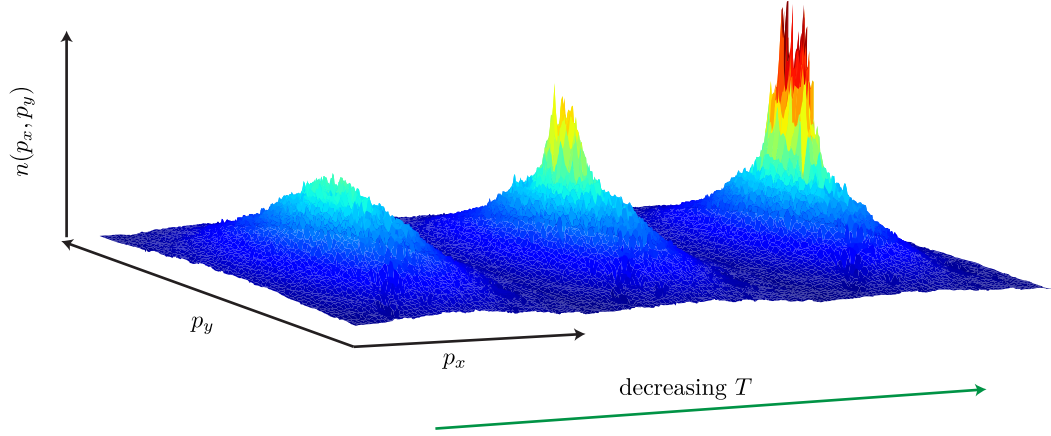


Figure 3: Momentum distribution of atoms near  $T_c$  after a 21 ms TOF. As the atoms are cooled below  $T_c$  a sharp peak in the momentum distribution appears indicating condensation.